PAPER Special Section on VLSI Design and CAD Algorithms

Extracting Device-Parameter Variations with RO-Based Sensors

Ken-ichi SHINKAI[†a)], ***Student Member***, **Masanori HASHIMOTO**[†b)], ***and*** **Takao ONOYE**[†c)], ***Members***

SUMMARY Device-parameter estimation sensors inside a chip are gaining its importance as the post-fabrication tuning is becoming of a practical use. In estimation of variational parameters using on-chip sensors, it is often assumed that the outputs of variation sensors are not affected by random variations. However, random variations can deteriorate the accuracy of the estimation result. In this paper, we propose a device-parameter estimation method with on-chip variation sensors explicitly considering random variability. The proposed method derives the global variation parameters and the standard deviation of the random variability using the maximum likelihood estimation. We experimentally verified that the proposed method improves the accuracy of device-parameter estimation by 11.1 to 73.4% compared to the conventional method that neglects random variations.

key words: *variation sensor, manufacturing variability, device-parameter, ring oscillator*

1. Introduction

Process variability is becoming more influential on circuit performance and parametric yield, and is predicted to get much severer as technology advances [1]. The process variability is often classified into D2D (Die-to-Die) and WID (WithIn-Die) variations. Especially, WID variation has been predicted to become more significant with device miniaturization [2].

To enhance the circuit performance after fabrication and improve parametric yield, several adaptation methods, such as voltage scaling and adaptive body bias, have been proposed [3], [4]. In order to adapt the performance efficiently, it is required to estimate for every chip how device-parameters varied from their typical values during the manufacturing process. For such a purpose, RO(Ring-Oscillator)-based sensors have been intensively studied [5]–[8]. They can be easily implemented in a chip and can be used to obtain variability information even after the product shipment, because the oscillating frequencies of ROs can be easily measured with a simple circuit structure. Conventional device-parameter extraction methods using RO-based sensors often assume that ROs are not affected by random variations because of the well-known averaging effect where the influence of random variation is assumed to be well suppressed by increasing the number of RO stages [9].

When implementing RO-based sensors using ordinary standard cells, the sensitivity vectors of the oscillation frequency to device parameters (e.g. channel lengths and threshold voltages for NMOS and PMOS) are close to each other, and it is difficult to accurately estimate device parameters. On the other hand, ROs that have high sensitivity to a single device-parameter have been proposed for decomposing the measured superposed variation into each device-parameter variation [7], [8]. However, when using such ROs, random variations might not be canceled out.

An example of this phenomenon is demonstrated here when using such a highly-sensitive RO to device-parameters. Figure 1 shows frequency distributions of 101-stage ROs composed of normal inverters or highly-sensitive inverters to NMOS parameters, which was obtained by Monte Carlo circuit simulation. The condition of this simulation is basically the same with that in Sect. 4, and will be explained later. Random variations of $\Delta V_{th_{n/p}}$ and $\Delta L_{n/p}$, whose averages are 0, are given, where $V_{th_{n/p}}$ means N/PMOS threshold voltage and $L_{n/p}$ is gate length of N/PMOS. ΔF denotes the shift of the oscillation frequency from its nominal value in an RO without any device-parameter variations, and ΔF is caused by device-parameter variations, such as $\Delta V_{th_{n/p}}$ and $\Delta L_{n/p}$. The number of samples for each distribution is 1,000, and then some non-smoothness appears in Fig. 1. When an RO comprises normal inverters, the average of ΔF is -0.45% and the standard deviation is 0.8%. On the other hand, when an RO consists of sophisticated inverters that have intentionally high

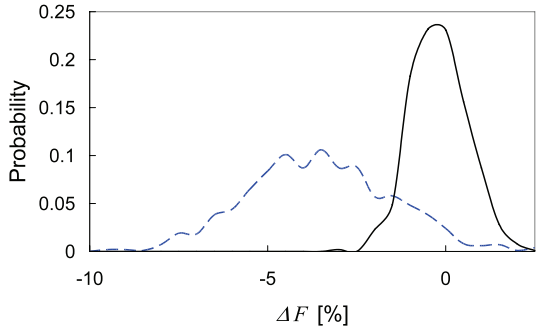

Fig. 1 Frequency-distributions with only random variations (without global variations). For each distribution, the number of sampled data is 1,000. Supply voltage is 0.9 V. Solid line denotes a distribution with an RO constructed by normal inverters (RO#1 in Sect. 4.1), and dashed line denotes that with an RO constructed by inverters that have high sensitivity to NMOS L and V_{th} (RO#2 in Sect. 4.1). The number of stages in both ROs is 101.

Manuscript received March 26, 2011.
Manuscript revised June 20, 2011.

[†]The authors are with the Department of Information Systems Engineering, Osaka University, Suita-shi, 565-0871 Japan.
a) E-mail: shinkai.kenichi@ist.osaka-u.ac.jp
b) E-mail: hasimoto@ist.osaka-u.ac.jp
c) E-mail: onoye@ist.osaka-u.ac.jp

DOI: 10.1587/transfun.E94.A.2537

sensitivity to device-parameters of ΔV_{th_n} and ΔL_n, the effect of random variability on ΔF is more significant. In fact, the random variability changes the average of ΔF by -3.8% even though the averages of every variation are 0. The standard deviation of ΔF reaches 2.0% indeed even when the number of RO stage is 101. Therefore, in order to accurately estimate device-parameters using such sophisticated ROs, random variability should be taken into account explicitly. Both the large standard deviation of ΔF and the shift of the average must be considered in the device-parameter estimation from the measured sensor outputs.

In this paper, we propose an estimation method of device-parameters, such as threshold voltage V_{th} and channel-length L of a transistor, explicitly considering the effect of random variability. This method is based on MLE (Maximum Likelihood Estimation) and extracts not only D2D parameter variations but also standard deviations of random variations. The accurate extraction and decomposition of N/PMOS device parameters contribute to an appropriate compensation with regard to both of performance and leakage-power consumption.

We also investigate the metric for sensor selection. A device-parameter could be estimated by a sensor that has a high sensitivity to a corresponding parameter. However, the sensitivities to other device parameters are not zero, and hence the estimated parameter must include some error. We take up three methods for selecting a set of sensors and compares them in terms of the estimation accuracy.

The rest of this paper is organized as follows. Section 2 presesents device-parameter extraction methods using RO-based variation sensor with and without the consideration of random variations. Section 3 explains three RO selection methods for evaluation. Section 4 shows experimental results, and finally Sect. 5 concludes this paper.

2. Parameter Extraction Methods Using RO-Based Variation Sensors

This section first explains parameter extraction methods without the consideration of the random variation effect, and proposes a parameter estimation method that explicitly takes into account the random variation.

In this paper, it is assumed that the variability is composed of two components, that are global and random variations for simplicity. Global is D2D variation which causes the same variation-offset to all transistors in a chip, while random corresponds to WID variation which is different transistor by transistor. Thus, an offset of a device-parameter x from its nominal value, ΔV_x, is expressed by Eq. (1),

$$\Delta V_x = \Delta G_x + \Delta R_x, \tag{1}$$

where ΔG_x denotes global variability, and ΔR_x corresponds to random variability of parameter x.

2.1 Parameter-Extraction Method without Consideration of Random Variations

A conventional parameter-extraction method assumes that the shift of the oscillation frequency from its nominal value in the i-th type of RO, ΔF_i, is expressed by Eq. (2),

$$\Delta F_i = \sum_x k_{i,x} \Delta G_x = \boldsymbol{k}_{\boldsymbol{i,x}}^{\mathrm{T}} \boldsymbol{\Delta G_x}, \tag{2}$$

where $k_{i,x}$ denotes the frequency-sensitivity to a variation of parameter x at RO#i. $\boldsymbol{k_{i,x}}$ and $\boldsymbol{\Delta G_x}$ are vector representations of $k_{i,x}$ and ΔG_x. Note that Eq. (2) can be extended to quadratic or higher-order model to improve the accuracy [10]. In this model, random variations are assumed to be canceled out and much smaller than global variations because of the averaging effect [9]. Therefore, none of ΔR_x appear in Eq. (2). Using Eq. (2), device-parameter variations are estimated by Eq. (3).

$$\boldsymbol{\Delta G_x} = \boldsymbol{K}^{-1} \boldsymbol{\Delta F} = \begin{pmatrix} \boldsymbol{k}_{\boldsymbol{1,x}}^{\mathrm{T}} \\ \vdots \\ \boldsymbol{k}_{\boldsymbol{n,x}}^{\mathrm{T}} \end{pmatrix}^{-1} \boldsymbol{\Delta F}. \tag{3}$$

At least n types of ROs should be used for the estimation of n parameters.

The device-parameter estimation in Eq. (3) assumes that every ΔR_x can be suppressed to be ignorable. However, as shown in Sect. 1, the averaging effect cannot completely exclude the effects of random variations. As the number of RO stages increases, the ratio of standard deviation to mean of oscillating frequency becomes smaller and it finally becomes ignorable. However, the shift of the average frequency observed in Fig. 1 cannot be eliminated even though the number of stages increases.

2.2 Parameter-Extraction Method Considering Random Variations

This subsection presents the proposed extraction method of device-parameters from the sensor outputs that include random variability. The proposed method defines a likelihood function, which tells how likely the measured frequencies are observed taking into account the effect of random variations shown in Fig. 1. We then obtain the most probable $\boldsymbol{\Delta G_x}$ and $\boldsymbol{\sigma_{\Delta R_x}}$ that maximize the likelihood function, i.e. most probably explain the measured frequencies. Here, $\sigma_{\Delta R_x}$ is the standard deviation of ΔR_x.

Figure 2 illustrates that the probability density function of ΔF_i changes according to $\boldsymbol{\Delta G_x}$ and $\boldsymbol{\sigma_{\Delta R_x}}$. Here, let us suppose that $p(\Delta F_i)$, i.e., the probability density function of ΔF_i, is expressed by a normal distribution. In other word, the distribution of the measured ΔF_i is assumed to follow $\mathrm{N}(\mu_{\Delta F_i}, \sigma^2_{\Delta F_i})$. Note that this method is independent of the shape of the assumed distribution and other distributions can be used depending on the actual data.

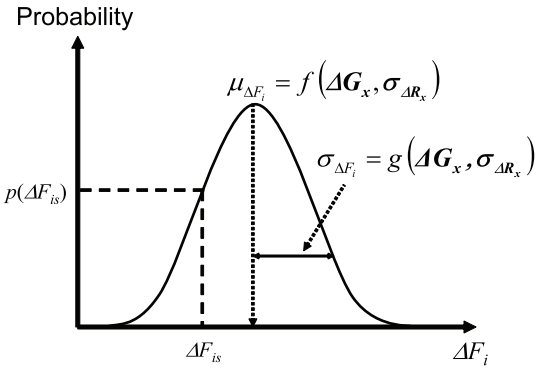

Fig. 2 Probability density function used for MLE.

$$\mu_{\Delta F_i} = f(\boldsymbol{\Delta G_x}, \boldsymbol{\sigma_{\Delta R_x}}), \tag{4}$$

$$\sigma_{\Delta F_i} = g(\boldsymbol{\Delta G_x}, \boldsymbol{\sigma_{\Delta R_x}}). \tag{5}$$

The base and order of functions f and g can be freely chosen to achieve the required accuracy. If we choose simple first-order approximation, for example, they are expressed by Eqs. (6) and (7),

$$\mu_{\Delta F_i} = \sum_x \left(a_{i,x}\Delta G_x + b_{i,x}\sigma_{\Delta R_x}\right), \tag{6}$$

$$\sigma_{\Delta F_i} = \sum_x \left(c_{i,x}\Delta G_x + d_{i,x}\sigma_{\Delta R_x}\right), \tag{7}$$

where $a_{i,x}$, $b_{i,x}$, $c_{i,x}$ and $d_{i,x}$ are coefficients.

When there are S_i sensor instances of RO#i in a chip, the likelihood function for independent and identically distributed samples of ΔF_i is expressed using $p(\Delta F_{is})$ by Eq. (8),

$$\prod_s^{S_i} p(\Delta F_{is}) = \prod_s^{S_i} \frac{1}{\sqrt{2\pi}\sigma_{\Delta F_i}} \exp\left(-\frac{(\Delta F_{is} - \mu_{\Delta F_i})^2}{2\sigma_{\Delta F_i}^2}\right), \tag{8}$$

where ΔF_{is} means the measured data from the s-th sensor instance of the i-th type of RO. If a device-parameter follows other type of distribution, the corresponding probability density function is used in Eq. (9) instead of Gaussian probability density function. When n types of ROs are used for estimation, we use the product of Eq. (8) as the overall likelihood function in this work.

$$\prod_i^n \prod_s^{S_i} p(\Delta F_{is}). \tag{9}$$

This overall likelihood function expresses how likely the measured frequencies are observed, and the function value varies depending on $\boldsymbol{\Delta G_x}$ and $\boldsymbol{\sigma_{\Delta R_x}}$ even for the same measured frequencies. By maximizing Eq. (9), we obtain the most probable $\boldsymbol{\Delta G_x}$ and $\boldsymbol{\sigma_{\Delta R_x}}$ that can explain the measured frequencies. The logarithm of Eq. (9) is expressed as Eq. (10), and it can be easily solved by any numerical computing environment.

$$\sum_i^n \sum_s^{S_i} \log(p(\Delta F_{is})) \tag{10}$$

3. RO Selection Methods

For accurate estimation of each device-parameter, it is important to carefully choose a set of RO sensors used for parameter estimation, referred to as ROset in the following. Sensitivity vectors of RO sensors, which correspond to $\boldsymbol{k_{i,x}}$ in Eq. (3), are used for the determination of RO design. In this paper, three selection methods are evaluated. The extraction results using ROsets obtained by each method will be discussed in Sect. 4.2.

3.1 SA (Sensitivity Amplitude)

A straightforward approach is to select ROs that have the highest sensitivity for each device-parameter and construct an ROset that includes the selected ROs. Here, $\mathrm{SA}_{i,x}$ (Sensitivity Amplitude) is defined as Eq. (11), which indicates how the sensitivity to x in RO#i dominates the sensitivities to the other parameters.

$$\mathrm{SA}_{i,x} = \frac{|k_{i,x}|}{\sum_{y \neq x} |k_{i,y}|}. \tag{11}$$

We choose n ROs in order that $\mathrm{SA}_{i,x}$s for each x are maximized.

3.2 ORTH (Orthogonality)

Reference [7] pointed out that when the sensitivity vectors are orthogonal, the estimation error decreases through an experiment of two-device-parameters estimation. On the basis of this idea, when all the sensitivity vectors are orthogonal to each other, the estimation result of $\boldsymbol{\Delta G_x}$ becomes more accurate. We derive an appropriate set of ROs with minimal RMSE (Root Mean Square Error) of angles between sensitivity vectors in Eq. (12).

$$\mathrm{RMSE\ (ROset)} = \sqrt{\frac{\sum_{\forall i \in (\mathrm{ROset})} \sum_{\forall j \in (\mathrm{ROset}), j \neq i} (angle_{ij} - 90^\circ)^2}{\binom{n}{2}}}, \tag{12}$$

where n is the number of ROs in an ROset and $angle_{ij}$ denotes an angle in degrees between the sensitivity vectors of RO#i and RO#j.

3.3 CON (Condition Number)

Reference [10] introduced another criterion, which is the condition number of a matrix. The condition number of a matrix $\boldsymbol{M}$, $cond(\boldsymbol{M})$, is defined mathematically as follows [11], [12],

$$cond(\boldsymbol{M}) = \|\boldsymbol{M}\|_\infty \cdot \|\boldsymbol{M}^{-1}\|_\infty. \tag{13}$$

$\|M\|_\infty$ is the infinity norm of $\boldsymbol{M}$ expressed in Eq. (14),

$$\|M\|_\infty = \max_{1\le i\le l} \sum_{j=1}^{n} |m_{ij}|, \tag{14}$$

where l and n are the numbers of rows and columns, respectively. m_{ij} denotes the entry that lies in the i-th row and the j-th column of the matrix. It is known that smaller condition number is, a better solution can be obtained in a numerical computation [12], such as Eq. (3). Additionally, smaller condition number is associated with a better orthogonality of row vectors in the matrix. Thus, CON is correlated with ORTH and might be a sort of a superset of ORTH. An appropriate ROset with this selection method is chosen by minimizing $cond(\boldsymbol{K})$.

4. Experimental Results

This section experimentally discusses the selection of a good set of sensors for device-parameter estimation. This section also verifies the accuracy enhancement of the proposed method compared to the conventional estimation. These evaluations are experimentally investigated using virtually-fabricated chips (simulated data). It is assumed that variation sources to be extracted are $V_{th_{n/p}}$ and $L_{n/p}$. Here, a commercial 65-nm process technology is used for evaluation.

4.1 Experimental Condition

As candidates for various ROs, eight ROs listed in Table 1 are chosen to evaluate sensitivity vectors. Diagrams of these circuits are illustrated in Appendix. The number of stages in all ROs is 101. Structures of RO#2–3 and RO#4–8 are similar with those in Refs. [7] and [8], respectively. The difference between RO#4 and RO#5 is sizes of each transistor. RO#8 consists of an inverting stage in the modified L-sensitive RO in Ref. [8] (Fig. A·5 in Appendix), while it is customized in order that four terminals (INVN/P and CAPN/P) are controllable to change the sensitivity vector (Fig. A·6 in Appendix). The experiment here assumes that selectable voltages at each terminal are V_{dd}, V_{bn}, V_{bp}, and V_{ss}, where V_{bn} and V_{bp} are generated by bias generators [8] (Fig. A·4 in Appendix). Therefore, 144 (= $3^2 4^2$) data can be obtained only using RO#8. The oscillating frequency of every RO could be measured at different V_{dd}s. The sensitivity vectors vary depending on V_{dd}, which means the number of ROs can be increased without consuming additional silicon area for sensors. In this experiment, 1.5, 1.2, and 0.9 V are used as V_{dd}. Equations (4) and (5) are modeled as second-order polynomials by fitting.

In what follows, it is assumed that $\sigma_{\Delta G/R_{Vth_{n/p}}}$ = 20 mV for transistors with L = 60 nm and W = 240 nm(NMOS)/360 nm(PMOS), and $\sigma_{\Delta G/R_{L_{n/p}}}$ = 2 nm. $\sigma_{\Delta G/R_{Vth_{n/p}}}$ were computed for each transistor taking into account the area dependency with Pelgrom's model [13]. According to the assumed process variability, virtually-fabricated chips were created with Monte Carlo approach and all sensor-outputs in each chip were evaluated with HSPICE [14].

Table 1 RO configuration.

RO No.	Component
1	Normal INV
2	INV followed by NMOS transistor
3	INV followed by PMOS transistor
4	INV followed by CMOS-controlled load - 1
5	INV followed by CMOS-controlled load - 2
6	Current-starved INV followed by PMOS-controlled load
7	Current-starved INV followed by NMOS-controlled load
8	Customized INV

4.2 Sensor Selection

The purpose in this section is to clarify which selection method is appropriate to derive an ROset that reduces the estimation error. The estimate accuracy is evaluated in the case that only global variations exist, i.e., $\sigma_{\Delta R_{Vth_{n/p}}} = \sigma_{\Delta R_{L_{n/p}}} = 0$. Thirty-five chips were virtually fabricated. Equation 4 with $\boldsymbol{\sigma_{\Delta R_x}} = \boldsymbol{O}$, i.e. zero matrix, is used for estimation.

The combinations of ROs that were selected by each selection method are shown in Table 2. Now four device-parameters are to be estimated and hence four ROs are basically selected. The best RMSE is 6.26° (ORTH), and the best condition number is 5.13 (CON).

Table 3 shows the averages of absolute estimation errors of $\boldsymbol{\Delta G_x}$. The results with ORTH is worse than those with SA and CON. The average errors of SA and CON, where each error is normalized by the corresponding stan-

Table 3 Average estimate errors of $\boldsymbol{\Delta G_x}$ under only global variations (the number of virtually-fabricated chips is 35).

Method	ΔG_{Vth_n} [mV]	ΔG_{Vth_p} [mV]	ΔG_{L_n} [nm]	ΔG_{L_p} [nm]
SA	0.22	0.61	0.29	0.10
ORTH	0.34	0.45	0.43	0.44
CON	0.28	0.29	0.13	0.24

Table 2 ROsets obtained by each selection method. Voltages enclosed by square brackets at RO#8 correspond to INVN, INVP, CAPN, and CAPP shown in Fig. A·6, in order from left to right.

Method	RO No. (V_{dd})	RO No. (V_{dd})	RO No. (V_{dd})	RO No. (V_{dd})
SA	2 (1.2)	3 (1.5)	8 [V_{dd}, V_{bp}, V_{bp}, V_{dd}] (1.5)	8 [V_{bn}, V_{ss}, V_{ss}, V_{ss}] (1.5)
ORTH	2 (0.9)	8 [V_{dd}, V_{bp}, V_{bp}, V_{dd}] (1.2)	8 [V_{bn}, V_{bp}, V_{bn}, V_{dd}] (1.5)	8 [V_{bn}, V_{ss}, V_{bp}, V_{bn}] (1.5)
CON	2 (1.5)	8 [V_{bn}, V_{bp}, V_{bp}, V_{dd}] (1.5)	8 [V_{bn}, V_{ss}, V_{ss}, V_{bn}] (1.5)	8 [V_{bp}, V_{bp}, V_{bn}, V_{bn}] (1.2)

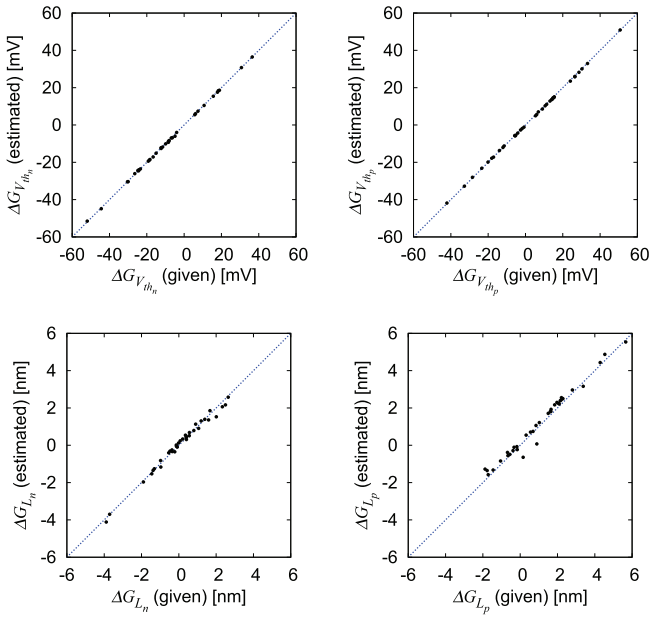

Fig. 3 Given $\Delta \boldsymbol{G_x}$ vs. estimated $\Delta \boldsymbol{G_x}$ with CON under only global variations. A dot corresponds to a result of a virtual chip.

dard deviation, are 5.9% and 5.3%, respectively. From the viewpoint of accuracy, the condition number is the best metric to select ROs in this experiment. This result suggests that the sensitivity matrix obtained with CON attains the most appropriate orthogonality and characteristics for numerical calculation.

Figure 3 illustrates scatter plots that compare estimated $\Delta \boldsymbol{G_x}$ with those given in virtual fabrication when using the ROset selected by CON. It shows that every ΔG_x is estimated with sufficient accuracy.

4.3 Importance of Considering Random Variation

This section evaluates the estimation accuracy when both global and random variations exist. Here it is demonstrated that neglecting random variability causes a significant degradation in accuracy. Five chips were virtually fabricated and each chip has 100 sensor instances for this evaluation. The proposed extraction method using MLE is compared with the conventional one that uses only Eq. (4) with $\boldsymbol{\sigma_{\Delta R_x}} = \boldsymbol{O}$, which means that the same model with the same accuracy was used for both the proposed and conventional methods, though the first-order model was used for simplifying the explanation of the conventional method in Sect. 2.1. Equations (4) and (5) are used for the proposed estimation and Eq. (9) is maximized to obtain $\Delta \boldsymbol{G_x}$ and $\boldsymbol{\sigma_{\Delta R_x}}$. To resolve Eq. (9), this experiment uses the *optim* function of R [15] with L-BFGS (Limited-Broyden-Fletcher-Goldfarb-Shanno) algorithm. Here the ROset obtained by CON is used for both methods.

Table 4 shows the averages of the absolute estimation errors of $\Delta \boldsymbol{G_x}$ from the given variations. Table 5 lists the average absolute errors of estimated $\boldsymbol{\sigma_{\Delta R_x}}$. These tables indicate that the proposed method reduces the estimate error by 11.1–73.4% and provides more accurate estimation thanks to the consideration of random variations.

Table 4 Absolute values of average estimate errors of $\Delta \boldsymbol{G_x}$ under global and random variations (the number of virtually-fabricated chips is five).

Method	ΔG_{Vth_n} [mV]	ΔG_{Vth_p} [mV]	ΔG_{L_n} [nm]	ΔG_{L_p} [nm]
Proposed	1.35	1.66	0.38	0.40
Conventional	4.01	6.23	0.57	0.45
Error reduction	66.3%	73.4%	33.3%	11.1%

Table 5 Average absolute errors of estimate of $\boldsymbol{\sigma_{\Delta R_x}}$ (the number of virtually-fabricated chips is five).

$\sigma_{\Delta R_{Vth_n}}$ [mV]	$\sigma_{\Delta R_{Vth_p}}$ [mV]	$\sigma_{\Delta R_{L_n}}$ [nm]	$\sigma_{\Delta R_{L_p}}$ [nm]
1.44	1.21	0.17	0.22

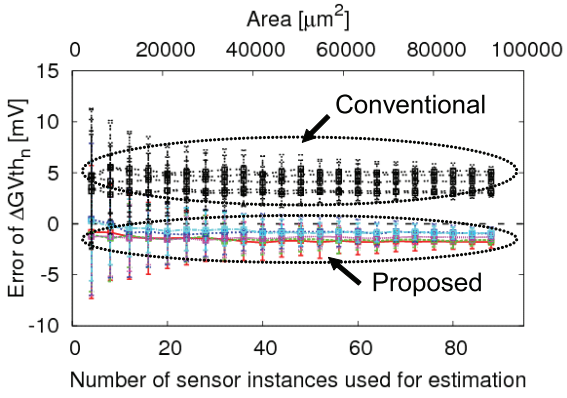

Fig. 4 The number of sensor instances vs. estimation error of $\Delta G_{V_{th_n}}$ (five chips). The upper axis corresponds to an area where the number of sensor instances in the bottom axis is used.

This section next demonstrates how the number of sensor instances, i.e., S_i in Eq. (9), affects the estimate accuracy. This evaluation is performed with the following process,

1. Make a set of sensor instances by randomly selecting those from 200 sensor instances on a virtually-fabricated chip,
2. Estimate variations using the above instance set,
3. Go back to step 1 until a pre-defined number of estimations are performed.

In this experiment, the pre-defined value in the third step above was 200, which means two hundred sets of sensor instances were generated for a die. The numbers of sensor instances evaluated here are 4–88 at four intervals.

Figure 4 illustrates the estimation errors of $\Delta G_{V_{th_n}}$ in five chips. Dots denote the average error, i.e., the expected error in 200 sets of S_i sensor instances, and error bars show the standard deviation of the average error. More sensor instances are used, more accurate the estimation result is. The standard deviation of the conventional method denotes the same tendency of that of the proposed method. However, the average error of the proposed method is smaller than that of the conventional method. Figure 5 shows the estimation

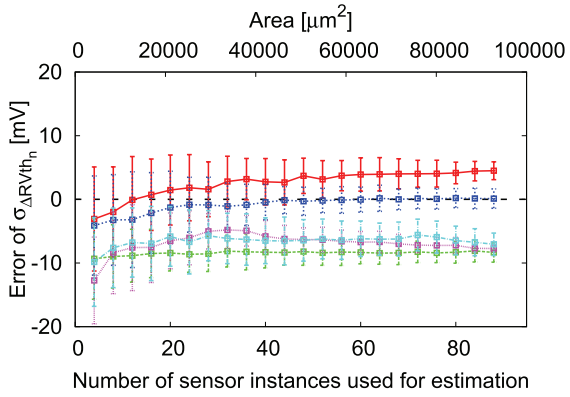

Fig. 5 The number of sensor instances vs. estimation error of $\sigma_{\Delta R_{V_{thn}}}$ (five chips). The upper axis corresponds to an area where the number of sensor instances in the bottom axis is used.

results of $\sigma_{\Delta R_{V_{thn}}}$ in five chips. Only the result with the proposed method is depicted, because the conventional method cannot estimate $\sigma_{\Delta R_{V_{thn}}}$. This figure indicates that the estimation results converge as the number of sensor instances increases. However, all of $\sigma_{\Delta R_{V_{thn}}}$ do not converge to zero error. A possible reason is that the ROset used in this experiment was derived with sensitivity matrix with respect to ΔG_x in Sect. 4.2, though the ROset derived with sensitivity matrix with respect to ΔG_x and $\sigma_{\Delta R_x}$ should be used. This is because computing sensitivity to $\sigma_{\Delta R_x}$ by Monte Carlo simulation is time-consuming, and computing sensitivity matrix for all ROs and RO configurations was not possible. A future work is to facilitate the sensitivity computation and derive a ROset with sensitivity matrix with respect to ΔG_x and $\sigma_{\Delta R_x}$.

5. Conclusion

This paper proposed a device-parameter estimation method with RO-based variation sensors in a chip. The proposed method takes into account random variability with maximum likelihood estimation. It was experimentally verified that the proposed method can accurately estimate variations, whereas disregarding random variability, which is often adopted in conventional methods, deteriorates the estimation accuracy of the global variation. This paper also investigated sensor selection methods, and showed that the RO selection based on the condition number of the sensitivity matrix provided the most accurate estimation in our test case.

Acknowledgments

This work is supported by New Energy and Industrial Technology Development Organization (NEDO). The authors would like to thank VLSI Design and Education Center (VDEC), the University of Tokyo in collaboration with Synopsys, Inc. This work is also supported by Grant-in-Aid for Scientific Research and JSPS Fellows.

References

[1] H. Masuda, S. Ohkawa, A. Kurokawa, and M. Aoki, "Challenge: Variability characterization and modeling for 65- to 90-nm processes," Proc. CICC, pp.593–599, 2005.
[2] H. Onodera, "Variability: Modeling and its impact on design," IEICE Trans. Electron., vol.E89-C, no.3, pp.342–348, March 2006.
[3] S. Martin, K. Flautner, T. Mudge, and D. Blaauw, "Combined dynamic voltage scaling and adaptive body biasing for lower power microprocessors under dynamic workloads," Proc. ICCAD. ACM, pp.721–725, 2002.
[4] J. Tschanz, J. Kao, S. Narendra, R. Nair, D. Antoniadis, A. Chandrakasan, and V. De, "Adaptive body bias for reducing impacts of die-to-die and within-die parameter variations on microprocessor frequency and leakage," IEEE J. Solid-State Circuits, vol.37, no.11, pp.1396–1402, 2002.
[5] M. Bhushan, M. Ketchen, S. Polonsky, and A. Gattiker, "Ring oscillator based technique for measuring variability statistics," ICMTS, pp.87–92, 2006.
[6] L. Pang and B. Nikolic, "Measurements and analysis of process variability in 90 nm CMOS," IEEE J. Solid-State Circuits, vol.44, no.5, pp.1655–1663, 2009.
[7] I.A.K.M. Mahfuzul, A. Tsuchiya, K. Kobayashi, and H. Onodera, "Process-sensitive monitor circuits for estimation of die-to-die process variability," Proc. TAU, pp.83–88, 2010.
[8] B. Wan, J. Wang, G. Keskin, and L.T. Pileggi, "Ring oscillators for single process-parameter monitoring," Proc. Workshop on Test Structure Design for Variability Characterization, 2008.
[9] D. Blaauw, K. Chopra, A. Srivastava, and L. Scheffer, "Statistical timing analysis: From basic principles to state of the art," IEEE Trans. Comput.-Aided Des. Integr. Circuits Syst., vol.27, no.4, pp.589–607, 2008.
[10] T. Takahashi, T. Uezono, M. Shintani, K. Masu, and T. Sato, "On-die parameter extraction from path-delay measurements," Proc. ASSCC, pp.101–104, 2009.
[11] J. Demmel, "On condition numbers and the distance to the nearest ill-posed problem," Numerische Mathematik, vol.51, no.3, pp.251–289, 1987.
[12] A. Bourdonnaye and M. Tolentino, "Reducing the condition number for microlocal discretization problems," Philosophical Trans. the Royal Society of London. Series A, vol.362, no.1816, pp.541–559, 2004.
[13] M.J.M. Pelgrom, A.C.J. Duinmaijer, and A.P.G. Welbers, "Matching properties of MOS transistors," IEEE J. Solid-State Circuits, vol.24, no.5, pp.1433–1439, Oct. 1989.
[14] HSPICE Documentation, Synopsys.
[15] R. [Online]. Available: http://www.r-project.org/

Appendix

Appendix shows schematics of RO components described in Table 1. Figures A· 1 and A· 3 illustrate those of RO#2, RO#4 (5) and RO#6. RO#3 and RO#7 are exact complementary circuits of RO#2 and RO#6, respectively. V_{bn} bias generator is shown in Fig. A· 4 and it is complementary of V_{bp} bias generator. As described in Sect. 4.1, RO#8 in Fig. A· 6 is based on Fig. A· 5. Here the characteristics of these circuits are described.

RO#2 component is sensitive to variations in NMOS. The size of NMOS path-transistor is smaller than each of transistor in inverting stage, and hence variation of the NMOS path-transistor have a dominant impact on this component.

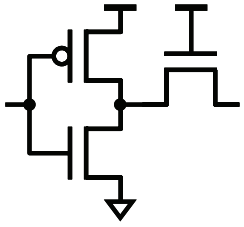

Fig. A· 1 RO#2 component: INV followed by NMOS transistor.

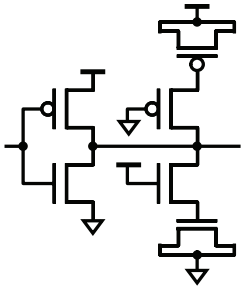

Fig. A· 2 RO#4 (5) component: INV followed by CMOS-controlled loads.

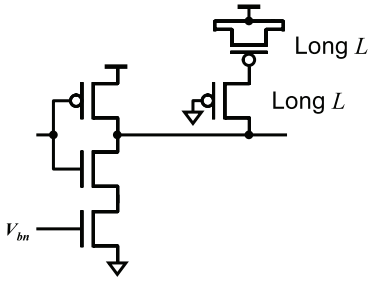

Fig. A· 3 RO#6 component: Current-starved INV followed by PMOS-controlled load.

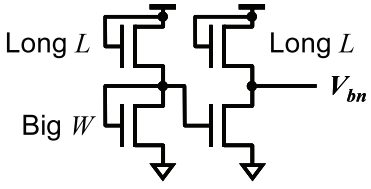

Fig. A· 4 V_{bn} bias generator for RO#6 and RO#8.

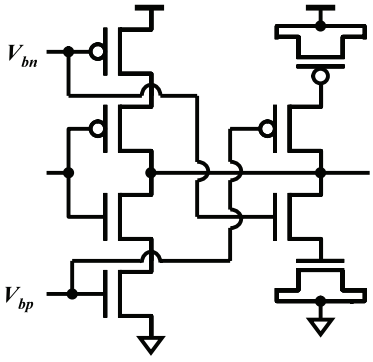

Fig. A· 5 Modified L-sensitive INV in Ref. [8].

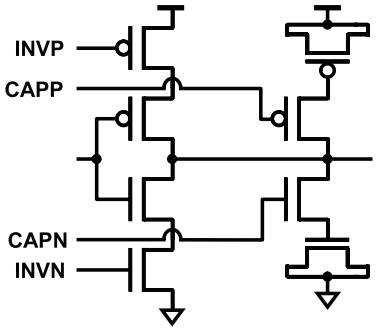

Fig. A· 6 RO#8 component: customized INV based on Fig. A· 5.

RO#4 (5) component gains the sensitivity to L. When V_{thn} increases, the inverting stage slows down. However at that time, NMOS load becomes smaller due to the increased effective resistance of NMOS. The two behaviors cancel each other out and the fall-propagation delay is insensitive to V_{thn}. Similar discussion is applicable to V_{thp}. Therefore, when the devices are properly sized, this component can become either L_n- or L_p-sensitive.

V_{bn} bias generator provides the voltage that is inversely proportional to V_{thn} and less dependent of L_n. The detailed description is omitted, but it should be noted that L and W of transistors are very important to attain this property. Considering PMOS-loading effect and V_{bn} bias generator, RO#6 component mitigates L and V_{thp} variations, and enhances the sensitivity to V_{thn} variation.

The structure in Fig. A· 5 is modified from that in Fig. A· 2. The authors of Ref. [8] observed that the structure in Fig. A· 2 does not provide a sufficient cancellation of V_{th} variations in 65-nm devices. Thus, they combined structures of Figs. A· 2 and A· 3. They switched the bias voltages for N/PMOS and obtained the opposite cancellation/amplification effects for L and V_{th} variations. RO#8 component in Fig. A· 6 is similar with Fig. A· 5, while four terminals (INVN/P and CAPN/P) can be set to V_{dd}, V_{bn}, V_{bp}, and V_{ss} to change the sensitivity to variations.

Ken-ichi Shinkai received the B.E. and M.E. degrees in Information Systems Engineering from Osaka University, Osaka, Japan, in 2006 and 2008, respectively. He is currently pursuing the Ph.D. degree in the Department of Information Systems Engineering at Osaka University. His major interest is variation-aware timing and reliability analysis. He is a student member of IEEE.

Masanori Hashimoto received the B.E., M.E. and Ph.D. degrees in Communications and Computer Engineering from Kyoto University, Kyoto, Japan, in 1997, 1999, and 2001, respectively. Since 2004, he has been an Associate Professor in Department of Information Systems Engineering, Graduate School of Information Science and Technology, Osaka University. His research interest includes computer-aided-design for digital integrated circuits, and high-speed circuit design. Dr. Hashimoto served on the technical program committees for international conferences including DAC, ICCAD, ASP-DAC, DATE, ISPD, ICCD and ISQED. He is a member of IEEE and IPSJ.

Takao Onoye received the B.E. and M.E. degrees in Electronic Engineering, and Dr.Eng. degree in Information Systems Engineering all from Osaka University, Japan, in 1991, 1993, and 1997, respectively. He is currently a professor in the Department of Information Systems Engineering, Osaka University. His research interests include media-centric low-power architecture and its SoC implementation. He is a member of IEEE, IPSJ, and ITE-J.